Available online at www.sciencedirect.com

jmr&t Journal of Materials Research and Technology

www.jmrt.com.br

Original Article

The enhancement of hydroxyapatite thermal stability by Al doping

M.A. Goldberg[a,*], P.V. Protsenko[b], V.V. Smirnov[a], O.S. Antonova[a], S.V. Smirnov[a], A.A. Konovalov[a], K.G. Vorckachev[a], E.A. Kudryavtsev[c], S.M. Barinov[a], V.S. Komlev[a]

[a] Baikov Institute of Metallurgy and Materials Science, Russian Academy of Sciences, 119334 Moscow, Russian Federation
[b] M. V. Lomonosov Moscow State University, 119991 Moscow, Russian Federation
[c] National Research University "Belgorod State University", 308015 Belgorod, Russian Federation

ARTICLE INFO

Article history:
Received 25 May 2019
Accepted 12 October 2019
Available online 14 November 2019

Keywords:
Al-substituted hydroxyapatite
Phase transformation
Thermal stability

ABSTRACT

Al-substituted hydroxyapatite (Al-HA) powders with apatite structure and particle size of 30–70 nm were obtained via precipitation method. The effect of Al content on specific surface area and morphology of powders was studied, and a formation of highly anisotropic phase due to Al doping was observed. The influence of heat treatment in 300–1400 °C range on the phase composition, lattice parameters, Fourier-transform infrared spectroscopy (FTIR) spectra and mass loss of powders was investigated. Introduction of Al in the hydroxyapatite (HA) lattice in the range 0.5–1.0 mol.% resulted in the improvement in thermal stability, which had not been reported previously. Incorporation of 5–10 mol.% of Al resulted in the formation of biphasic materials based on HA and whitlockite-like structure at 900 °C and apatite and α- tricalcium phosphate (α-TCP) phases at 1200–1400 °C. Introduction of 20 mol.% of Al resulted in the formation of isomorphic Al-substituted whitlockite phase $Ca_9Al(PO_4)_7$. We have estimated the onset of $Ca_9Al(PO_4)_7$ transformation into α-TCP phase at 1400 °C.

1. Introduction

Hydroxyapatite (HA) is one of the most attractive biomaterials for bone reconstruction due to its good biological compatibility and osteoconductivity [1]. Introduction of different cations into HA structure can lead to beneficial effects on biomaterial properties such as the degree of structural order (i.e. crystallinity), morphology, mechanical properties, degradability, and dissolution rate under physiological conditions. Cation-substituted HA is known to provide many advantages for reconstructive surgery and bone tissue engineering applications [2]. Introduction of different cations into HA structure influences its behavior during heat treatment. Thermal stability of HA depends on several factors, including particle size, Ca/P ratio, and water vapor pressure. Available data on the HA

Abbreviations: HA, hydroxyapatite; Al-HA, Al-substituted hydroxyapatite; FTIR, Fourier-transform infrared spectroscopy; α-TCP, α-tricalcium phosphate; β-TCP, β-tricalcium phosphate; XRD, X-ray diffraction; AES-ICP, atomic emission spectrometry with inductively coupled plasma; FEG SEM, field emission gun scanning electron microscopy; TEM, transmission electron microscopy; ED, electron diffraction; S, specific surface area; TG, thermogravimetry.

* *Corresponding author.*
E-mail: mgoldberg@imet.ac.ru (M. Goldberg).

https://doi.org/10.1016/j.jmrt.2019.10.032

thermal stability are controversial: according to Wang et al. decomposition of HA with the formation of β-tricalcium phosphate (β-TCP) begins at 1100 °C [3], while HA stability of HA up to 1250 °C was reported in [4]. HA rapidly lose water under vacuum starting from 850 °C [5] which was confirmed by the decrease of intensity of corresponding FTIR bands and detection of α-TCP peaks at 1000 °C by X-ray diffraction (XRD) [3].

Thermal stability of HA depends significantly upon the substitution of calcium by other cations and phosphate by halogens [6]. Specifically, mono- and divalent cations substitution was investigated in Refs. [7,8], due to their significant influence on the structure, properties and thermal behavior of HA and β-TCP ceramic materials. Incorporation of sodium did not deteriorate the HA phase stability up to 900 °C [9]. Increased thermal stability of the potassium substituted hydroxyapatites and biphasic mixtures of HA/β-TCP till 1300 °C without any phase decomposition was revealed [10]. Introduction of Mn in the HA structure resulted in a decrease of decomposition temperature: incorporation of 5 wt.% of Mn resulted in the onset of decomposition at 800 °C with complete transformation into α-TCP and Mn_3O_4 occurringat 1250 °C [11]. The decrease of thermal stability was also observed for Zn [12], Ni [13], and Cd [14] substituted HA. Influence of transition metal cations on thermal stability has been extensively studied for HA coatings on the Ti surface. The interaction between HA and Ti leads to a significant decrease of decomposition temperature, with the formation of the α-TCP at 900 °C [4].

The effect of trivalent metal ions has been studied in detail for Fe (III) substituted HA [15]. The formation of β-TCP at 800 °C was detected in all compounds with Fe concentration above 0.7 at.%. There are some data on the effect of Bi, La, Y and In substitution on thermal stability of HA and osteoblast response [16,17].

The reports on the influence of Al on HA structure, phase composition, and thermal behavior are limited. Nie et al. synthesized aluminum substituted hydroxyapatite (Al-HA) powders by coprecipitation method and obtained nanoparticles without any impurity phases in as-synthesized materials [18]. Similarly, Wakamura et al. obtained pure Al-HA nanoparticles by coprecipitation and ion-exchange methods and reported that Al inhibits dental caries [19]. However, in these studies, thermal stability of substituted HA has not been investigated. The sol-gel synthesis of Al-HA followed by heat treatment at 900 °C was unsuccessful above 10 at.%: phase mixtures of $AlPO_4$, CaP_4O_{11}, $Al_3(PO_4)_2(OH)_3(H_2O)_5$ and $Ca_2Al(PO_4)_2(OH)$ were obtained [20]. Kolekar et al. synthesized aluminum doped HA by solution combustion method with subsequent annealing at 950 °C: the powders were biphasic and contained HA and a small amount of Al_2O_3. Obtained samples did not have toxic effects on cell lines L929 [21].

The biocompatibility of aluminum contained HA is regarded a controversial question, which requires further investigation. The increased aluminum content in drinking water had been linked with the brain dementia including Alzheimer disease [22]. However, this assumption was criticized in later research [23], where no change in bulk aluminum content in the human brains of healthy people and Alzheimer disease patients was demonstrated and proven. In the same time, aluminum hydroxide and aluminum phosphate are considered as the important immune adjuvants approved by the FDA for use in humans due to its safety and efficacy [24–27]. Composite materials based on hydroxyapatite and Al_2O_3 containing clinoptilolite obtained by high-temperature sintering at 1300 °C demonstrated biocompatibility and absence of acute toxicity for SAOS-2 cells [28].

There are several potential applications of Al-HA outside the field of bioceramics. For example, Al-HA is reported to be an efficient adsorbent material for water purification [18]. The nanoscale powders of Al-HA are proposed as a drug career system [21]. Also, HA can serve as coating on the Al_2O_3 [29,30] or $Ti_6Al_{14}V$ substrates: its interaction with substrate materials could result in the Al-HA formation at high temperature [31]. Ceramics based on HA and Al_2O_3 possess enhanced mechanical properties [32]. Viswanath Ravishankar have demonstrated the formation of Ca aluminates in HA-Al_2O_3, but the heat treatment was limited by 1000–1200 °C [33].

This work is aimed at the investigation of the influence of Al content on the phase composition, morphology and thermal stability of powders obtained by precipitation method over the wide range of aluminum content up to 20 mol.% substitution.

2. Experimental

Powder synthesis was carried out according to reaction 1 via precipitation method using reactants of analytical grade (LTD Labtech, Russia) and deionized water.

$$(10\text{-}x)Ca(NO_3)_2 + 6(NH_4)_2HPO_4 + (2x/3)Al(NO_3)_3 + 8NH_4OH \rightarrow$$

$$Ca_{(10-x)}Al_{2x/3}(PO_4)_6(OH)_2 + 20NH_4NO_3 + 6H_2O, \quad (1)$$

$$x = 0; 0.005; 0.01; 0.05; 0.1; 0.2$$

Calcium and aluminum nitrate salts were mixed with 250 ml deionized water to obtain the solutions with selected ratios (Table 1). The solutions of a diammonium hydrogen phosphate were prepared with 150 ml deionized water. The diammonium hydrogen phosphate solution were added by dropping to calcium and aluminum nitrate solution withthe mixing during 1 h at the room temperature. The pH of the reaction mixture was maintained at a level of 9.0–9.5 by adding aqueous ammonia. Powders were ripened at mother solution during 21 days at the temperature of 25 °C for full crystallization of precipitate [34]. The obtained powders were filtered, washed and dried at 60 °C for 24 h. The powders were heat-treated at 300 °C for 3 h in air to remove the ammonium nitrate, an impurity phase. Then the powders were heat-treated in the air for 3 h at T = 900 °C, 1200 °C, and 1400 °C. Further, the materials were ground in an agate mortar to a powder with the particle size under 100 μm.

For determination of Al content in the precipitates, powders were dissolved in HCl–HNO3 mixture and analyzed by inductively coupled plasma atomic emission spectroscopy (HORIBA Jobin Yvon, ULTIMA 2) (ICP-AES). Field emission gun scanning electron microscopy (FEG SEM) assessed the particle morphology of synthesized powders (CrossBeam 1540 EsB, Carl Zeiss, gold sputtered specimens in scanning electron microscope mode, accelerating voltage of 7 kV, 5 mm WD, 30 μm aperture size) and by transmission electron microscopy

Table 1 – Initial reagent ratio, powder composition and surface area.

Ca substitution by Al, mol.%	Stoichiometric formulae	m $Ca(NO_3)_2{*}4H_2O$, g	m $Al(NO_3)_3{*}9H_2O$, g	m $(NH_4)_2HPO_4$, g	Al theoretical, mol.%	Al theoretical, wt.%	Al measured, wt.%	S, m^2/g
0	$Ca_{10}(PO_4)_6(OH)_2$	58.76	0.00	19.72	0	0	$<10^{-4}$	91(3)
0,5	$Ca_{9,95}Al_{0,033}(PO_4)_6(OH)_2$	58.54	0.31	19.74	0.5	0.086	0.082 (0.003)	53(2)
1	$Ca_{9,9}Al_{0,066}(PO_4)_6(OH)_2$	58.31	0.62	19.77	1.0	0.173	0.17(0.02)	71(3)
5	$Ca_{9,5}Al_{0,33}(PO_4)_6(OH)_2$	56.46	3.14	19.95	5	0.876	0.84(0.03)	73(3)
10	$Ca_9Al_{0,66}(PO_4)_6(OH)_2$	54.11	6.35	20.18	10	1.772	1.79(0.03)	84(3)
20	$Ca_8Al_{1,33}(PO_4)_6(OH)_2$	49.23	13.01	20.65	20	3.629	3.62(0.04)	90(3)

TEM (JEOL JEM 2100, carbon sputtered specimens, accelerating voltage of 200 kV, 1000 mm of the diffraction length, 25.1). The parameters of lattice and phase composition were determined by the electron diffraction (ED) obtained by TEM. The specific surface area (S) of the as-synthesized powders was determined by low-temperature nitrogen adsorption measurements (BET, Micromeritics TriStar analyzer). The powder materials were characterized by the XRD method (Shimadzu XRD-6000, CuKα radiation, step = 0,02°) with identification of phase composition according to ICDD PDF database. The lattice parameters of HA, β – TCP, α – TCP and $Ca_9Al(PO_4)_7$ (as a phase with the whitlockite-like structure similar to β – TCP) were determined by Rietveld refinement method using the GSAS/EXPGUI software package [35,36]. The Rietveld refinements were performed with fixed structural parameters of the $P6_3/m$ structural model of partially substituted HA [37]. The model provides moderately acceptable fit quality for all datasets: reliability factors for the 1% of Al 900 °C sample are $R_p = 13.3\%$, $R_{wp} = 20.3\%$. However, to confirm the absence of systematic error which might be caused by imperfect fit of intensities, structureless (Le Bail) fit was also performed at one model composition, and the refined values of lattice parameters coincided within 1 e.s.d. Consequently, the lattice for all other compositions were evaluated by Rietveld method only as it provided superior computational stability.

Fourier-transform infrared spectroscopy (FTIR) analysis has been performed with a Nikolet Avatar FTIR spectrometer and spectra have been obtained in the range from 4000 to 400 cm^{-1} to evaluate the functional group of the specimens. Thermogravimetry (TG) data were obtained in a Netzsch STA 409 Luxx simultaneous thermal analysis system during continuous heating from 25 to 1400 °C under air flow, without holding at any fixed point temperatures. An empty crucible was used as a reference. The heating rate was 10 °C/min. The composition of the gases released during thermal decomposition was determined by mass spectrometry using a Netzsch QMS 403 C Aëolos quadrupole mass spectrometer with a capillary inlet system.

3. Results

3.1. *Powders chemical composition, morphology and surface area*

Data on the Al content in the powders as determined by ICP-AES are presented in Table 1, the chemical composition of synthesized materials is close to the nominal one.

Formation of Al-HA powders structure was observed in pH 9–9.5 media formed by aqueous ammonia solution. In spite of Al amphoteric properties, we assumed the formation of $Al(OH)_3$ in the aqueous ammonia solution media according to Ref. [38]. $Al(OH)_3$ does demonstrate the acid behavior in the alkali conditions of NaOH (pH > 12), but does not dissolve in ammonia solution (pH 10–11) and could not form $[Al(OH)_4]^-$ [39]. The formation of HA structure occurred during the ripening in the mother solution without $[Al(OH)_4]$- anions and incorporation of $[Al(OH)_4]$- in the HA structure in this conditions seems unlikely. In the same time, we did not observe $[AlO_4]^-$ bands in the FTIR spectra of as-synthesized powders

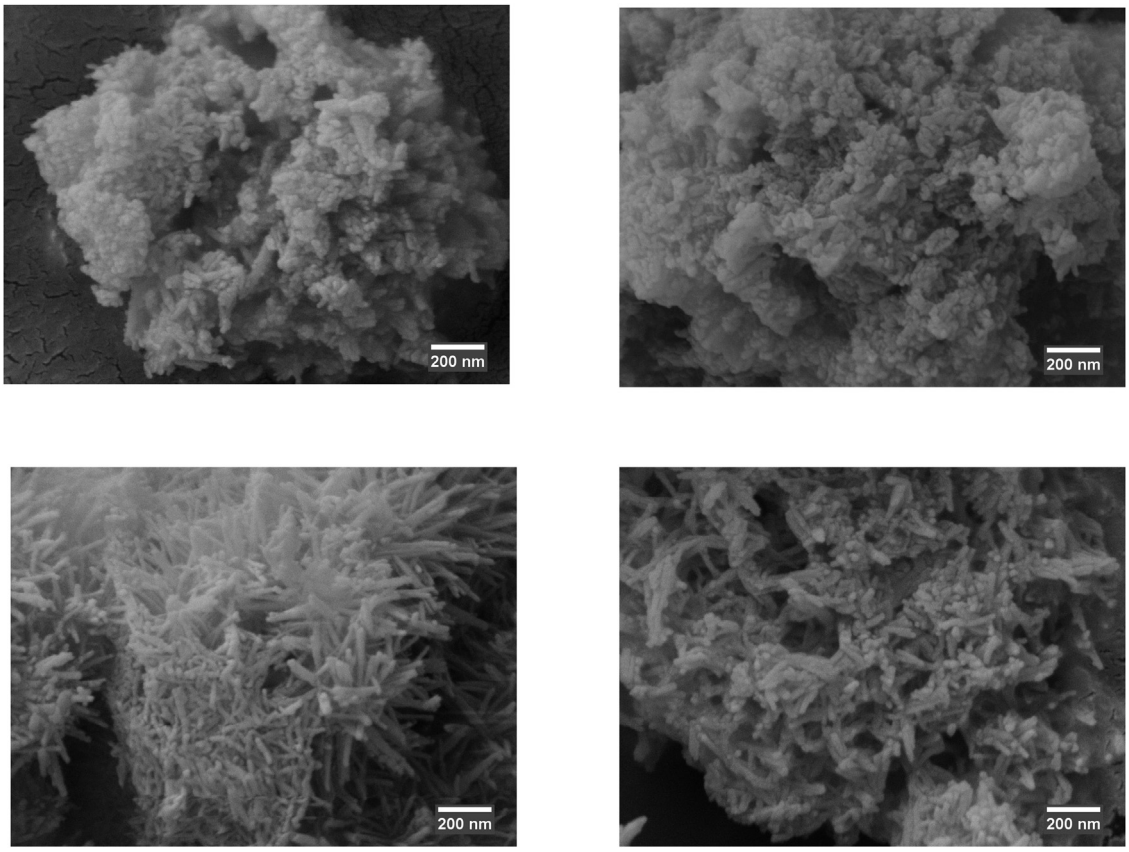

Fig. 1 – As synthesized precipitates before heat — treatment (FEG SEM), a — 0 mol.% of Al; b — 0.5 mol.% of Al; c — 1.0 mol.% of Al; d — 10 mol.% of Al. 2.

and samples heat-treated at low temperature. As-synthesized $Al(OH)_3$ had amorphous structure and preserved chemically active state. Its Al^{3+} cation participated in the formation of HA structure during the ripening and heat treatment.

According to FEG SEM and TEM data, as synthesized pure HA materials appeared as agglomerates of uniaxial and prismatic particles with average sizes of 20–30 nm (Fig. 1a). Materials with 0.5 mol.% of Al formed compact agglomerates consisted of spherical particles slightly larger than 30–50 nm with broad size distribution (Fig. 1b). As Al content increases up to 1 mol.%, the particle morphology evolved toward the formation of 70–100 nm length and ~10 nm in diameter needle-like crystals and remained almost unchanged with the further increase of Al content (Fig. 1c, d). The TEM data confirmed FEG SEM observations and evolution from predominantly round-shaped and irregular-shaped to needle-like and prismatic particles was observed with increase of Al content (Fig. 2). The similar shape changes of as-synthesized by precipitation method HA particles with substitution up to 10 mol. % of Al has been described in Ref. [19].Thus, doping of HA by Al provoke the formation of highly anisotropic phase.

According to N_2 absorption data, the pure as-synthesized HA had the specific area S (BET) of 91 m^2/g. The introduction of Al resulted in a noticeable decrease of S down to 53 m^2/g. This effect may be connected with the changes in particle size and morphology due to the increase of spherical particles diameter as detected by microscopy (see above). Additionally, the decrease of S can be connected with the change of agglomerates density. (Table 1).

Further increase of Al concentration has resulted in a gradual increase of S up to 90 m^2/g for 20 mol.% of Al due to formation of needle-like particles with twice lower thickness compared to the diameter of spherical particles.

3.2. *Powder TEM ED data and XRD*

According to TEM ED data, the as-synthesized powder of pure HA presented in Fig. 2a were formed by the apatite phase (PDF #9-432) with interplanar spacing (d value) of the most intense reflections of $d_1 = 3.48$ Å (002); $d_2 = 3.13$ Å (102); $d_3 = 2.78$ Å (112). The introduction of 0.5 mol.% of Al resulted in formation of HA phase with slightly decreased values of d, with the corresponding ED reflections at $d_1 = 3.34$ A (002) and d2 = 3.14 Å (102) and d3 = 2.77A(112). The increase of Al content up to 1 mol.% did not result in any distinguishable changes in the diffraction patterns compared to 0.5 mol.% (Fig. 2b, c). Similarly, the EED of materials with 10 mol. of Al % revealed the only phase of HA with $d_1 = 3.34$ Å (002), $d_2 = 3.06$ Å (102), $d_3 = 2.78$ Å (112) (Fig. 2d). No additional lines were observed indicating the absence of impurity phases.

According to the XRD analysis, all powders preheated at 300 °C consisted of apatite-like phases with a low degree of crystallinity; the peak width increased with Al content growth, confirming the data of Ref. [40] (Fig. 3a). The only detected

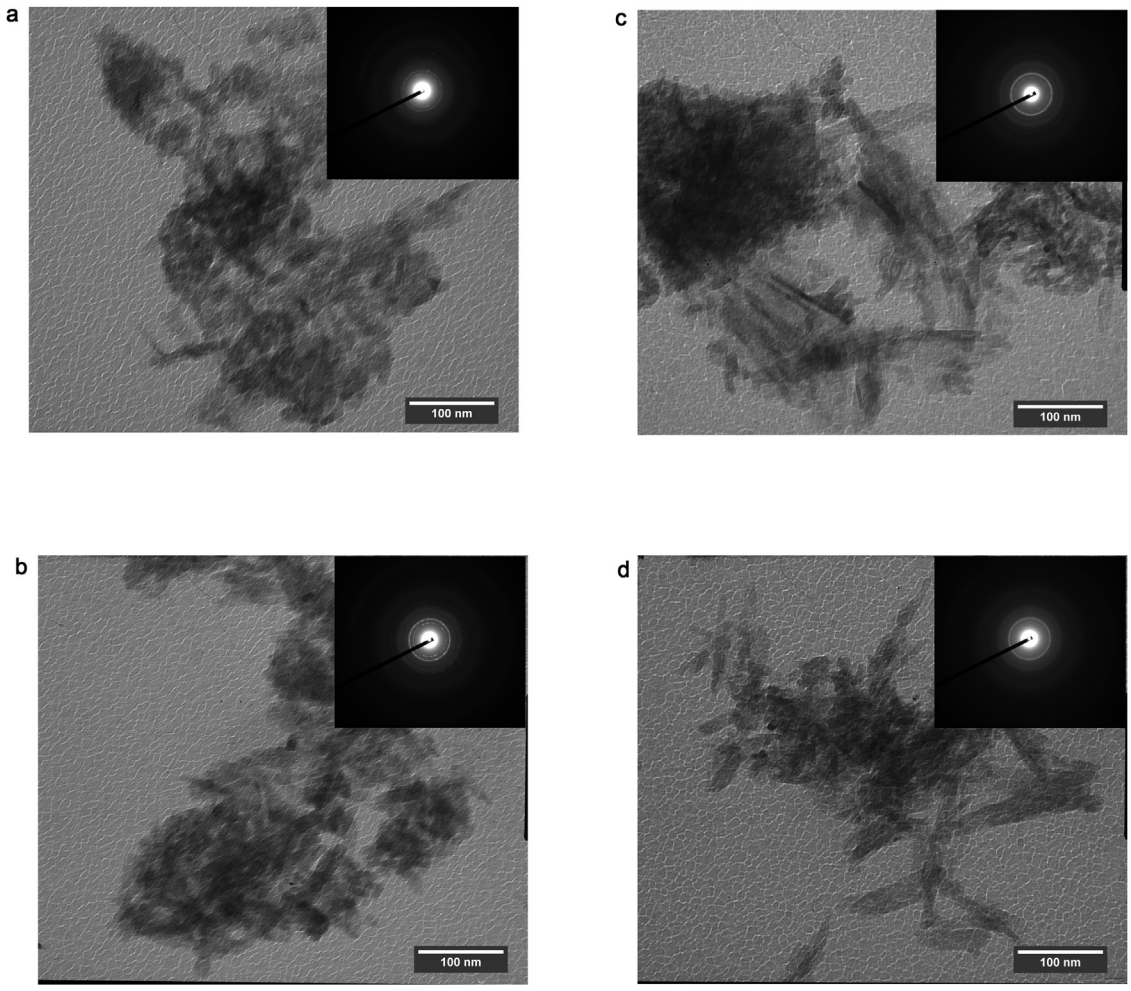

Fig. 2 – TEM investigations of powders before heat — treatment, a — 0 mol.% of Al; b — 0.5 mol.% of Al; c — 1.0 mol.% of Al; d — 10 mol.% of Al.

phase in all these samples was hydroxyapatite (PDF #9-432) consistent with the electron diffraction data of as-synthesized powders. The shape of triplet between 30,5° and 33,5° became smoother and transformed into the doublet for the sample containing 20 mol.% of Al.

After the heat treatment at 900 °C the degree of crystallinity of powders increased significantly (Fig. 3b). For Al content below 1 mol.% the only detected phase was HA (Table 2), with the position of main peaks shifted toward larger diffraction angles indicating the decrease of unit cell parameters. Formation of β-TCP (PDF # 09–0169) phase was detected starting from 5 mol.% of Al. We attribute the formation of β-TCP in the samples containing more than 1 mol.% of Al to the limited solubility of Al in HA lattice and starting of dehydration processes confirmed by FTIR and TG data. Further increase of Al content up to 20 mol.% resulted in the full transformation of HA to the whitlockite-like phase. In our previous work on the Al-substituted β-TCP, we had demonstrated the partial transformation of β-TCP into $Ca_9Al(PO_4)_7$ (PDF # 48-1192) with Al doping and further co-existence of these two phases [41]. Here, XRD data do not allow to determine the phase composition unambiguously due to broad peaks and strong overlap - hence, we further assumed the existence of the only Al-contained whitlockite-like phase - β-TCP observed with HA at 5–10 mol. % of Al; however the presence of some $Ca_9Al(PO_4)_7$ could not be excluded. At 20 mol.% of Al $Ca_9Al(PO_4)_7$ was the only detected phase. Reflections corresponded to $AlPO_4$ (PDF # 72-1161) and Al_2O_3 (PDF # 83-2081) were not detected in all compositions. Refined lattice parameters of β-TCP for materials with 5–10 mol.% of Al and of $Ca_9Al(PO_4)_7$ at 20 mol.% of Al are summarized in Table 3.

The heat treatment at 1200 °C resulted in a partial transformation of pure HA (0 mol.% of Al) into β-TCP (about 10 wt.%) due to dehydroxylation of HA structure (as discussed below in connection with FTIR observations) in agreement with literature data [42]. At the same time, the diffraction patterns of materials with 0.5 and 1.0 mol.% contained only reflections of HA without traces of β-TCP. Transformation of HA into the high-temperature modification – α-tricalcium phosphate (α-TCP) (PDF # 29-359) was observed for materials with 5 and 10 mol.% of Al (Fig. 3c). The amount of α-TCP in the resulting mixture was estimated as 65 wt.% and 87 wt.% for 5 and 10 mol.% of Al respectively. Formation of α-TCP for powder with 20 mol.% of Al was not observed, due to stabilization of Al-

Table 2 – Phase composition.

Ca substitution by Al, mol.%	300 °C	900 °C		1200 °C			1400 °C		
	$Ca_{10}(PO_4)_6(OH)_2$ wt. %	$Ca_{10}(PO_4)_6(OH)_2$ wt. %	β-$Ca_3(PO_4)_2$ wt. % ($Ca_9Al(PO_4)_7$[a])	$Ca_{10}(PO_4)_6(OH)_2$ wt. %	α-$Ca_3(PO_4)_2$ wt. %	β-$Ca_3(PO_4)_2$ wt. % ($Ca_9Al(PO_4)_7$[a])	$Ca_{10}(PO_4)_6(OH)_2$ wt. %	α-$Ca_3(PO_4)_2$ wt. %	β-$Ca_3(PO_4)_2$ wt. % ($Ca_9Al(PO_4)_7$[a])
0	100	100	0	90	0	10	72	28	0
0.5	100	100	0	100	0	0	80	20	0
1.0	100	100	0	100	0	0	88	12	0
5	100	78	22	35	65	0	44	56	0
10	100	63	37	13	87	0	6	94	0
20	100	0	100	0	0	100	0	5	95

[a] β-$Ca_3(PO_4)_2$ transformed into $Ca_9Al(PO_4)_7$ when 20 mol.% of Al was introduced.

Table 3 – Lattice parameters in nanometers.

Ca substitution by Al. mol.%	900 °C				1200 °C							1400 °C						
	$Ca_{10}(PO_4)_6(OH)_2$		β-$Ca_3(PO_4)_2$ ($Ca_9Al(PO_4)_7$)[a]		$Ca_{10}(PO_4)_6(OH)_2$		α-$Ca_3(PO_4)_2$			β-$Ca_3(PO_4)_2$ ($Ca_9Al(PO_4)_7$)[a]		$Ca_{10}(PO_4)_6(OH)_2$		α-$Ca_3(PO_4)_2$			β-$Ca_3(PO_4)_2$ ($Ca_9Al(PO_4)_7$)[a]	
	a	c	a	c	a	c	a	b	c	a	c	a	c	a	b	c	a	c
0	0.9416(3)	0.6883(4)			0.9423(3)	0.6884(5)				1.0431(5)	3.7384(4)	0.9427(3)	0.6910(2)	1.5257(2)	2.7418(5)	1.2863(2)		
0.5	0.9410(2)	0.6874(3)			0.9421(4)	0.6885(2)						0.9414(2)	0.6902(1)	1.5219(4)	2.7281(2)	1.2886(4)		
1.0	0.9408(4)	0.6860(2)			0.9425(2)	0.6889(4)						0.9416(4)	0.6887(3)	1.5219(2)	2.7282(3)	1.2885(4)		
5	0.9417(6)	0.6872(2)	1.0392(4)	3.7360(2)	0.9427(3)	0.6894(5)	1.5235(4)	2.7364(6)	1.2859(2)			0.94133(5)	0.6916(4)	1.5231(3)	2.7379(1)	1.2856(2)		
10	0.9435(6)	0.6879(4)	1.0400(2)	3.7403(3)	0.9305(6)	0.6892(3)	1.5238(2)	2.7359(3)	1.2861(5)			0.9417(7)	0.6886(6)	1.5239(4)	2.7344(2)	1.2866(5)		
20			1.0339(3)	3.7340(6)						1.0364(4)	3.7432(2)			1.5220(4)	2.7280(4)	1.2886(3)	1.0372(2)	3.7388(3)

[a] β-$Ca_3(PO_4)_2$ transformed into $Ca_9Al(PO_4)_7$ when 20 mol.% of Al was introduced.

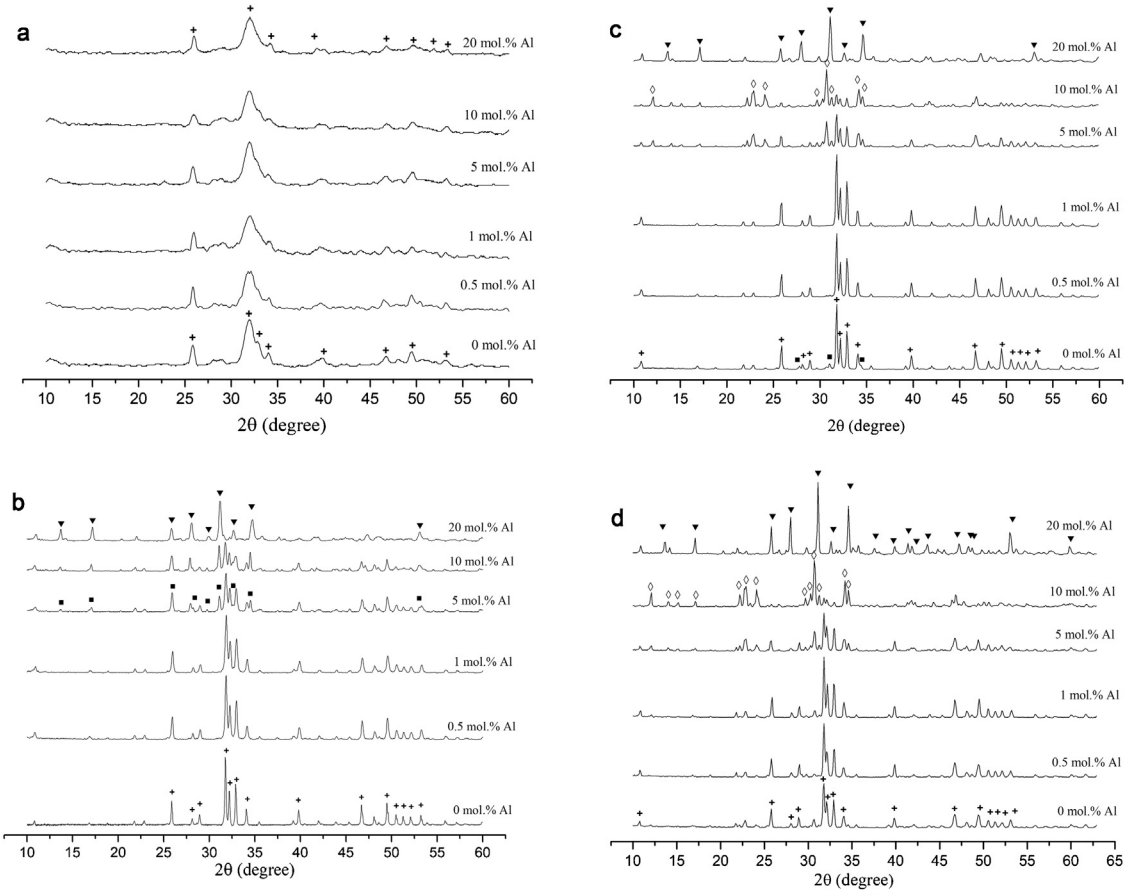

Fig. 3 – XRD spectra of Al — HA powders: + — HA (PDF No: 9 -432), ■ — β-TCP (PDF No: 09–0169), ▼ — $Ca_9Al(PO_4)_7$ (PDF No: 48-1192), ◊ — α-TCP (PDF No: 29-359); a — 300 °C; b — 900 °C; c — 1200 °C; d — 1400 °C.

enriched $Ca_9Al(PO_4)_7$ phase [43]. No reflections corresponding to any additional phases were detected.

Formation of α-TCP in all compositions including pure HA occurred at 1400 °C. Similar to the data on 1200 °C treatment described above, samples with 0.5 and 1.0 mol.% Al-HA demonstrated higher amount of HA and a lower content of α-TCP phase compared to pure HA (Fig. 3d). The increase of Al content above 5 mol.% resulted in a growth of α-TCP content, which reached 94 wt.% for the 10 mol.% of Al. Traces of α-TCP and whitlockite-like phase $Ca_9Al(PO_4)_7$ were detected in a material with 20 mol.% of Al,indicating that $Ca_9Al(PO_4)_7$ starts to transform into α-TCP between 1200 and 1400 °C. The temperature of this transformation was not reported in the literature up to date. No other crystalline phases including calcium aluminates or AlPO4 were detected in our samples.

Unit cell parameters were calculated for HA, β-TCP, $Ca_9Al(PO_4)_7$ and α-TCP as a function of composition and annealing temperature presented in Table 3. Decrease of Al-HA cell parameters at 900 °C for concentration 0.5–1.0 mol.% of Al could be interpreted as a formation of solid solution due to introduction of Al^{3+} with lower ionic radii comparing to Ca^{2+} (0.051 and 0.104 nm respectively) into the HA lattice [44], but the observed magnitude of the effect is close to the detection limit of the XRD method (0.6860 compared to 0.6883 nm).

According to the density functional theory simulation of Wang [40] the most stable Al-HA structure of $Ca_{8.5}Al(PO_4)_6(OH)_2$ should demonstrate the decrease of parameter *a* in order of 0.001 nm and parameter c in order of 0.003 nm with respect to pure HA. We have obtained the same order of magnitude changes in lattice parameters refined from XRD data, justifying the formation of solid solution in the case of low Al concentration. We have attempted also to confirm the formation of the solid solution from the electron diffraction data of as-synthesized powders, but the resolution of the method was insufficient to reveal relatively small changes of cell parameters.

It is difficult to interpret unambiguously the observed increase of lattice parameters at >5 mol. % Al content (Table 3). This effect could be attributed to the formation of amorphous Al-rich phase on the surface of the grains. Starting from 5 mol.% of Al β-TCP phase formed along with initial HA, with cell parameters independent on Al content. As the amount of Al increases up to 20 mol. %, the Al-enriched whitlockite-like phase $Ca_9Al(PO_4)_7$ formed. This phase had significantly lower lattice parameters comparing to β-TCP. At 1200 °C formation of HA structure with lattice parameters close to theoretical ones (PDF #9-432) was observed. The difference between cell parameters of pure HA and Al-substituted HA was within the margin of error. Thus, XRD could not reveal definitely where Al was located — either in a solid solution based on HA structure or in a separate amorphous phase at the grain surfaces. After the heat treatment at 1400 °C, a slight decrease of cell

Table 4 – Matched FTIR peaks presented at spectra (Fig.4) at different temperature.

Peak assignment	Temperature/wavenumber				
	60 °C	300 °C	900 °C	1200 °C	1400 °C
Structural OH	3565, 631 cm^{-1}	3565, 631 cm^{-1}	3570, 631 cm^{-1}	3569, 632 cm^{-1}	3571, 631 cm^{-1}
H_2O adsorbed	3510–2832, 1639 cm^{-1}	3510–2832, 1639 cm^{-1}	3510–2870, 1694–1561 cm^{-1}		
CO_3^- group (ν_3)	1444–1416 cm^{-1}	1444–1416 cm^{-1}			
CO_3^- group	871 cm^{-1}	871 cm^{-1}			
NO_3^- group	1385, 820 cm^{-1}	1385, 820 cm^{-1}			
PO_4 bend ν_3	1089, 1044 cm^{-1}	1089, 1044 cm^{-1}	1092, 1044 cm^{-1}	1083, 1024 cm^{-1}	1170–981 cm^{-1}
PO_4 stretch ν_1	962 cm^{-1}	962 cm^{-1}	961 cm^{-1}	962 cm^{-1}	963 cm^{-1}
PO_4 bend ν_4	607, 568 cm^{-1}	607, 568 cm^{-1}	602, 572 cm^{-1}	602, 573 cm^{-1}	606, 572 cm^{-1}
PO_4 bend ν_2	468 cm^{-1}	468 cm^{-1}	467 cm^{-1}	471 cm^{-1}	486–461 cm^{-1}
P-O-P				828 cm^{-1}	832 cm^{-1}
HPO_4^{2-}			890	895	

parameters was observed similar to samples treated at 900 °C. Moreover, this effect was masked by partial dehydration of HA which was reported to influence on cell parameters [45].

Only in the case of β-TCP phase formation of Al-substituted crystal structure of 20 mol. % of Al samples was confirmed by the refined values of cell parameters, which were close to one reported for $Ca_9Al(PO_4)_7$ [46].

3.3. *FTIR investigations*

The bands presented in the spectra of powders heated at different temperatures are listed in Table 4. The FTIR spectral bands of as-synthesized powders were wide due to amorphous state of powders and characterized by the presence of adsorbed H_2O, OH^-, PO_4^{3-}, NO_3^- and CO_3^- groups (Fig. 4a). The impurity anion bands of NO_3^- at 820 and 1380 cm^{-1} were attributed to residual nitrate groups resulting from nitrate synthesis precursors and traces of the impurity synthesis product phase NH_4NO_3 [47]. The absorption bands at 1419 and 875 cm^{-1} could be linked with the presence of CO_3- in the HA structure adsorbed from the air during the synthesis [48]. The small peak of the stretching vibration of OH^- at 3570 cm^{-1} and a slight librational band of OH^- at 635 cm^{-1} indicated the formation of the HA structure with low crystallinity and decreased in their intensity with the increase of Al amount. Adsorbed H_2O appeared in the spectra by broadened regions at 2900–3400 cm^{-1} and 1780–1525 cm^{-1}. The phosphate group was detected by significantly broadened peaks of stretching vibration modes ν_1 at 962 cm^{-1} and ν_3 region at 1170 cm^{-1}, and 980 cm^{-1}, by doublet at 562, and 602 cm^{-1} from the P—O bending mode ν_4, and by the slight triplet at 420–480 cm^{-1} of doubly generate bending mode ν_2 [49]. The absence of the bands at 840, 808, and 784 cm^{-1} which could be attributed to the stretching vibrations mode of Al—O in AlO_4 and 727, 690, and 646 cm^{-1} associated with those in AlO_6 groups confirmed the introduction of Al as the cation substitute [50,51].

The spectra of powders heat-treated at 300 °C are similar to the spectra of as-synthesized ones, but with better resolution (Fig. 4b). Additionally, the intensity of NO_3^- bands at 820 and 1380 cm^{-1} decreased due to the removal of traces of NH_4NO_3 during the heat-treatment. The presence of librational and stretching weak bands of OH^- at 635 and 3572 cm^{-1} indicated the formation of the HA structure for all compositions including the 20 mol.% of Al.

The FTIR bands of powders after heat treatment at 900 °C are further improved in resolution reflecting the more crystallized structure of powders (Fig. 4c). The FTIR spectra of specimens with 0–1.0 mol.% of Al well corresponded to typical FTIR spectra of HA after heat treatment at 900 °C [52]. The intensity of $NO_3^-$and CO_3^{2-} bands decreased dramatically and almost disappeared for all samples. As the amount of Al increased, the librational and stretching band of OH^- at 635 and 3572 cm^{-1} became sharp, and gradually decreased in their intensity. For 10 mol% of Al the librational band noticeably diminished and for 20 mol.% of Al disappeared completely due to the formation of β-TCP. The bands related to the phosphate group of ν_1- ν_2 for materials 0–1.0 mol.% of Al were narrow and appeared at 570, 602, 1034 and 1086 cm^{-1} with broadening during further increase of Al content. For materials with 20 mol.% of Al a broad band of ν_3 $PO_4^{3-}$was observed in the region of 1200–950 cm^{-1} attributed to the structure of β-TCP [53]. The new band of at 890 cm^{-1} was assigned to HPO_4^{2-}. The absence of ν_2 CO_3^{2-} mode with the same wavenumber (890 cm^{-1}) is confirmed by the absence of absorption in the region 1545–1410 cm^{-1} where the much stronger ν_3 bands would be seen [54]. Thus, heat treatment at 900 °C resulted in the formation of the HA structure of materials 0–1.0 mol.% of Al. Further increase of Al content stimulated formation of β-TCP due topartial dehydration of HA structure. This was confirmed by the appearance of the bands at 945 and 1025 cm^{-1} corresponding to oxyhydroxyapatite (OHA) functional group [55].

After the heat treatment at 1200 °C the OH^- bands observed at 3572 and 635 cm^{-1} were the most intense for the sample containing 0.5 mol.% of Al. The intensity of OH^- bands drops significantly over the concentration of 1.0 mol.% (Fig. 4d). Similar to the situation with the 900 °C heat-treated samples, this indicated the process of dehydroxylation in the HA structure with the formation of OHA. The detection of OHA by XRD is difficult due to overlapping of the characteristic peaks [6]. The transformation of HA into α-TCP is confirmed by the broadening of pure HA characteristic bands of PO_4^{3-} group in the range 1175–950 cm^{-1}, which extended up to 1200–950 cm^{-1}. The band at 830 cm^{-1} observed at 5–20 mol.% of Al could be attributed to the formation of asymmetric stretching P—O—P

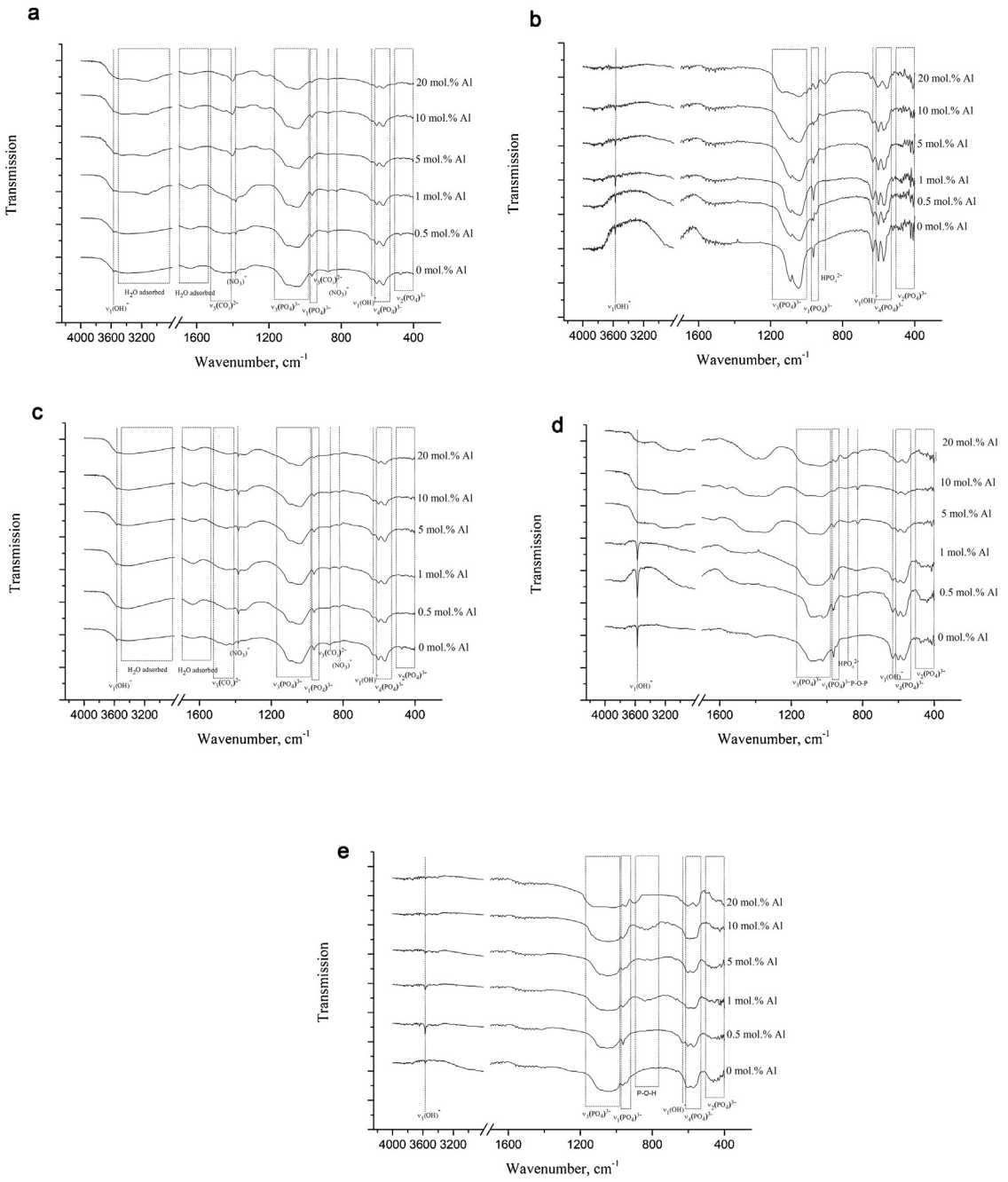

Fig. 4 – FTIR spectra of Al - HA heated at different temperatures, a — 60 °C, b — 300 °C, c — 900 °C; d — 1200 °C; e — 1400 °C.

bond of P_2O_5 [56] The band of HPO_4^{2-} at 885 cm^{-1} demonstrated splitting analogous to the one described in Ref. [54].

At 1400 °C, the spectra of pure HA showed the disappearance of the librational band of OH^- at 635 cm^{-1} and a presence of a very slight stretching band at 3572 cm^{-1} (Fig. 4e). The introduction of Al in low concentration up to 1.0 mol.% resulted in the stabilization of HA structure as indicated by the increase of intensity for both librational and stretching OH- bands, in agreement with XRD data. The bands corresponding to PO_4^{3-} groups demonstrated the broadening tendency with the increase of Al content. With the increase in the Al content, the absorption band ν_2 PO_4-group shifted toward higher wavenumbers from 461 to 486 cm^{-1}. The broadband region with low intensity at 720–880 cm^{-1} at 10–20 mol.% of Al can be assigned to the asymmetric stretching P—O—P [57].

3.4. *Thermogravimetry*

According to the mass-spectroscopy data, the main emitted substance during the heating up to 1400 °C was H_2O (18 *m/z*); additionally some N_2O (44 *m/z*) was detected at temperature below 900 °C as a product of NH_4NO_3 traces decomposition [58]. TG curves of the powders in the temperature range of 400–1400 °C were presented in Fig. 5. The mass of samples

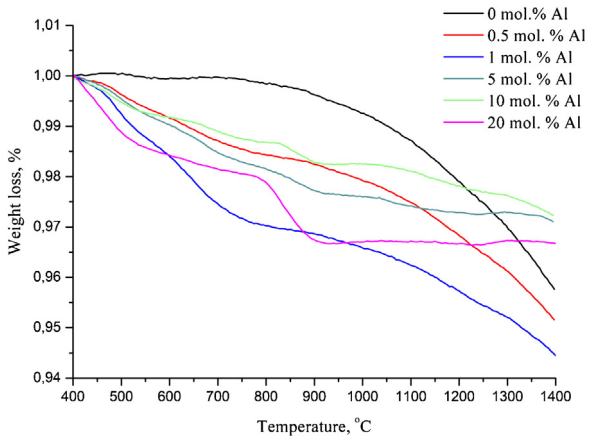

Fig. 5 – TGA curves of Al - HA heated from 400 to 1400 °C.

have been normalized on the mass at 400 °C (after the loss of adsorbed water). HA and Al-HA have high adsorption capacity [59]. The addition of Al increases the adsorption capacity due to formation of Al—OH surface groups in addition to the surface P—OH as discussed by Wakamura et al. [19].

Pure HA did not show noticeable mass loss in the temperature range of 400–900 °C, crystallization of HA was the main process as confirmed by XRD. The HA phase started to lose the structure water after 900 °C and demonstrated increase of dehydroxylation rate with temperature growth, confirmed by the decrease of OH^- bands intensity in FTIR spectra (1.70% in the range of 900–1200 °C compared to 2.55% in the range of 1200–1400 °C). The first stage of mass loss of samples with 0.5–1.0% of Al was observed in the temperature range of 400–900 °C and can be linked with the removal of N_2O and additional adsorbed water preserved by Al—OH surfaces (1.75% and 3.12%, respectively). The intensity of regions corresponding to adsorbed water (3505-2800 cm^{-1} and 1690-1535 cm^{-1}) on FTIR spectra at 300 °C were remarkably higher compared to pure HA and had the highest intensity for the sample with 1.0 mol.% of Al. Samples with 0.5 and 1.0 mol.% of Al demonstrated TG patterns similar to the one for pure HA at the temperature above 900 °C. The mass loss of 1.38% and 1.13% respectively was linked with desorption of physically absorbed water. According to XRD and FTIR data on OH^- band at 3572 cm^{-1}, these samples consisted of the apatite phase up to 1200 °C, and started to lose the structural water in the 1200–1400 °C temperature range. For 5 and 10 mol.% of Al the mass loss up to 900 °C was linked with the removal of traces of N_2O, adsorbed water and structural OH^-. The samples with 5 and 10 mol.% of Al demonstrate considerable increase in mass loss at 820 °C which could be attributed to the onset of the thermal decomposition of amorphous HA with the formation of β-TCP. As the 5 mol.% of Al preserved the higher amount of Al-HA according to XRD at 900 °C, the additional effect of adsorbed water is higher compared to 10 mol.% of Al and the corresponding mass losses to 900 °C constituted 2.29% and 1.73%, respectively. The further gradual mass loss at higher temperatures was linked with transformation of Al-HA into TCP structures as confirmed by a decrease of the OH^- bands intensity in FTIR spectra compared to OH^- bands in the pure HA.

The sample with 20 mol.% of Al lost the dominant amount of adsorbed water to 400 °C, which was confirmed by FTIR at 300 °C and mass-spectroscopy data. This sample demonstrated acceleration of mass loss at 780 °C attributed to transformation of amorphous HA into β-TCP and the loss of all water to 900 °C. According to XRD data and the absence of H_2O and OH^- bands at FTIR spectra at 900 °C, this correlates with the complete transformation of amorphous Al-HA into β-TCP.

4. Discussion

By means of the synthesis precipitation method, we obtained apatite phases at 300 °C and calcium phosphate Al-substituted phases for all Al contents (0–20 mol.%) at 900, 1200 and 1400 °C. According to FTIR data, there were no aluminates in obtained powders [60].

We investigated the kinetics of phase transformations and processes of dehydration of these Al-doped powders as a function of Al content and temperature. The influence of Al on the dehydration of HA observed in our experiments could be summarized in the schematic Fig. 6. We have plotted the amount of crystallized apatite phase – HA and OHA in the samples after heat treatment at 900, 1200 and 1400 °C. For each amount of Al, the predictive line of phase composition depending on temperature was drawn. It could be seen that a small amount of Al (0.5–1.0 mol.%) stabilizes apatite phase and the effect seems to be more pronounced in the case of lowest concentration – 0.5 mol.%. In the same time, addition of more than 5 mol. % of Al facilitate the formation of TCP phases. For 20 mol. % of Al complete transformation of HA into β-TCP was observed at a temperature less than 900 °C. This result is confirmed by FTIR spectra and TG curve. Such complex behavior was observed for the first time.

Stabilization of the HA phase by a small amount of Al – 0.5 and 1.0 mol. % is the most interesting and unexpected result of our work. This result was demonstrated by both XRD data (Table 2) and marked differences in FTIR spectra for 1200 and 1400 °C. Previous studies observed the destabilization of HA due to the introduction of a high amount of Al at high temperature [20,33] and did not discuss the influence of a small amount of Al on the HA stability. The reason for this stabilization is the formation of Al solid solution based on HA or formation of an amorphous phase on the grain surface. The changes of lattice parameters and broadening of HA peaks at 0.5–1.0 mol.% of Al are indications of solid solution formation, but peaks broadening also could be interpreted as a decrease of crystalline size of HA. Formation of Al – containing amorphous phase could not be detected by XRD analysis, and consequently, this point needs more detailed investigations. FTIR data demonstrated that high amount of Al led to the dehydration of powders and in the same time the presence of low amount of Al resulted in a conservation of OH^- groups on the surface of Al-HA compared to pure HA.

It is logical to claim that the incorporation of Al could decreased the transformation rate at low concentration. This effect is connected with a noticeable decrease of specific surface area due to the introduction of a low amount of Al (from 91

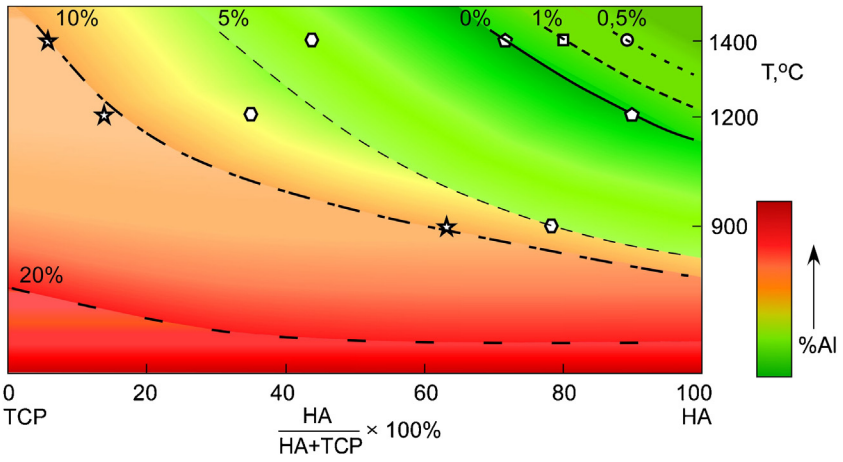

Fig. 6 – The schematic curves of the apatite phase amount (HA + OHA) in the mixture depending on the initial Al concentration.

to 53 m^2/g): which would tend to slow down the dehydration of HA.

Thus, both thermodynamic and kinetic aspects are able to stabilize HA phase at high temperature in the presence of a low amount – 0.5–1.0 mol.% of Al. This result allows to improve the methodology of high-temperature synthesis of HA-based coatings for Al-containing subtracts ($Ti_6Al_{14}V$) due to an increase of HA thermal stability [31].

5. Conclusions

Al-substituted HA powders with apatite structure and crystallite size of 30–70 nm were obtained by precipitation method. Introduction of Al in the HA lattice over the substitution range 0.5–1 mol.% resulted in the stabilization of the HA structure at high temperature. The increase of thermal stability due to the introduction of Al at low concentration was not reported previously. Introduction of 5–10 mol.% of Al resulted in the formation of biphasic materials based on HA and whitlockite-like structure at 900 °C and apatite and α-TCP phases at 1200–1400 °C. Introduction of 20 mol.% of Al resulted in the formation of isomorphic Al-substituted whitlockite phase $Ca_9Al(PO_4)_7$. We estimated the onset of $Ca_9Al(PO_4)_7$ transformation into α-TCP phase at 1400 °C. This result allows to increase the sintering temperature of Al-HA and produce high-temperature coatings with fixed phase composition.

Conflicts of interest

The authors declare no conflicts of interest.

Acknowledgments

The authors would like to thank the Russian Foundation for Basic Research for financial support under the grant No. 18-29-11053. The FEG SEM investigations were partly financially supported by State Assignment no 075-00746-19-00.

The authors thank A. A. Fomina from the Baikov Institute of Metallurgy and Materials Science for performing the ICP-AES investigations.

REFERENCES

[1] Aoki H. Science and medical applications of hydroxyapatite. Ishiyaku Euroamerica; 1991.
[2] Barinov SM. Calcium phosphate-based ceramic and composite materials for medicine. Russ Chem Rev 2010;79:13–29.
[3] Wang PE, Chaki TK. Sintering behavior and mechanical-properties of hydroxyapatite and dicalcium phosphate. J Mater Sci Med 1993;4:150–8.
[4] Weng J, Liu X, Zhang X, Ji X. Thermal decomposition of hydroxyapatite structure induced by titanium and its dioxide. J Mater Sci Lett 1994;13:159–61.
[5] Trombe JC, Montel G. Some features of the incorporation of oxygen in different oxidation states in the apatitic lattice-I on the existence of calcium and strontium oxyapatites. J Inorg Nucl Chem 1978;40:15–21.
[6] Tõnsuaadu K, Gross KA, Pluduma L, Veiderma M. A review on the thermal stability of calcium apatites. J Therm Anal Calorim 2012;110(2):647–59.
[7] Matsumoto N, Sato K, Yoshida K, Hashimoto K, Toda Y. Thermal stability of β-tricalcium phosphate doped with monovalent metal ions. Mater Res Bull 2009;44:1889–94.
[8] Goldberg MA, Smirnov VV, Antonova OS, Shvorneva LI, Smirnov SV, Kutsev SV, et al. Heat treatment-induced phase transformations of materials in a system of calcium phosphates and magnesium phosphates with (Ca + Mg)/P = 2. Inorg Mater 2016;52:1121–5.
[9] Sopyan I, Pusparini E, Ramesh S, Tan CY, Ching YC, Wong NIZ, et al. Influence of sodium on the properties of sol-gel derived hydroxyapatite powder and porous scaffolds. Ceram Int 2017;43:12263–9.
[10] Kannan S, Ventura JMG, Ferreira JMF. Synthesis and thermal stability of potassium substituted hydroxyapatites and hydroxyapatite/β-tricalciumphosphate mixtures. Ceram Int 2007;33:1489–94.
[11] Paluszkiewicz C, Ślósarczyk A, Pijocha D, Sitarz M, Bućko M, Zima A, et al. Synthesis, structural properties and thermal

stability of Mn-doped hydroxyapatite. J Mol Struct 2010;976:301–9.
[12] Li M, Xiao X, Liu R, Chen C, Huang L. Structural characterization of zinc-substituted hydroxyapatite prepared by hydrothermal method. J Mater Sci Mater Med 2008;19:797–803.
[13] Guerra-Lpez J, Poms R, Della Vdova CO, Via R. Influence of nickel on hydroxyapatite crystallization. J Raman Spectrosc 2001;32:255–61.
[14] Nounah A, Lacout JL. Thermal behavior of cadmium-containing apatites. J Solid State Chem 1993;107:444–51.
[15] Kaygili O, Dorozhkin SV, Ates T, Al-Ghamdi AA, Yakuphanoglu F. Dielectric properties of Fe doped hydroxyapatite prepared by sol-gel method. Ceram Int 2014;40:9395–402.
[16] Buvaneswari G, Varadaraju UV. Synthesis and characterization of new apatite-related phosphates. J Solid State Chem 2000;149:133–6.
[17] Webster TJ, Massa-Schlueter EA, Smith JL, Slamovich EB. Osteoblast response to hydroxyapatite doped with divalent and trivalent cations. Biomaterials 2004;25:2111–21.
[18] Nie Y, Hu C, Kong C. Enhanced fluoride adsorption using Al (III) modified calcium hydroxyapatite. J Hazard Mater 2012;233:194–9.
[19] Wakamura M, Kandori K, Ishikawa T. Surface structure and composition of calcium hydroxyapatites substituted with Al(III), La(III) and Fe(III) ions. Colloids Surf A Physicochem Eng Asp 2000;164:297–305.
[20] Kaygili O, Tatar C, Yakuphanoglu F, Keser S. Nano-crystalline aluminum-containing hydroxyapatite based bioceramics: synthesis and characterization. J Solgel Sci Technol 2013;65:105–11.
[21] Kolekar TV, Thorat ND, Yadav HM, Magalad VT, Shinde MA, Bandgar SS, et al. Nanocrystalline hydroxyapatite doped with aluminium: a potential carrier for biomedical applications. Ceram Int 2016;42:5304–11.
[22] Perl DP. Relationship of aluminum to Alzheimer's disease. Environ Health Perspect 1985;63:149–53.
[23] Alexander J, Gronnesby JK, Bakketeig LS, Edwardson JA. Content of brain aluminum is not elevated in Alzheimer disease. Alzheimer Dis Assoc Disord 1996;10:171–4.
[24] Montomoli E, Piccirella S, Khadang B, Mennitto E, Camerini R, De Rosa A. Current adjuvants and new perspectives in vaccine formulation. Expert Rev Vaccines 2011;10(7):1053–61.
[25] Zhu FC, Meng FY, Li JX, Li XL, Mao QY, Tao H, et al. Efficacy, safety, and immunology of an inactivated alum-adjuvant enterovirus 71 vaccine in children in China: a multicentre, randomised, double-blind, placebo-controlled, phase 3 trial. Lancet 2013;381(9882):2024–32.
[26] Liu H, Jia Z, Yang C, Song M, Jing Z, Zhao Y, et al. Aluminum hydroxide colloid vaccine encapsulated in yeast shells with enhanced humoral and cellular immune responses. Biomaterials 2018;167:32–43.
[27] Morefield GL, Sokolovska A, Jiang D, Hogenesch H, Robinson JP, Hem SL. Role of aluminum-containing adjuvants in antigen internalization by dendritic cells in vitro. Vaccine 2005;23:1588–95.
[28] Kalkandelen C, Suleymanoglu M, Kuruca SE, Akan A, Oktar FN, Gunduz O. Part 2: biocompatibility evaluation of hydroxyapatite-based clinoptilolite and Al_2O_3 composites. J Aust Ceram Soc 2017;53(1):217–23.
[29] Jiang G, Shi D. Coating of hydroxyapatite on highly porous Al_2O_3 substrate for bone substitutes. J Biomed Mater Res 1998;43:77–81.
[30] Shi D, Jiang G, Wen X. In vitro bioactive behavior of hydroxylapatite-coated porous Al_2O_3. J Biomed Mater Res 2000;53:457–66.
[31] van Dijk K, Schaeken HG, Wolke JCG, Marée CHM, Habraken FHPM, Verhoeven J, et al. Influence of discharge power level on the properties of hydroxyapatite films deposited on Ti_6A1_4V with RF magnetron sputtering. J Biomed Mater Res 1995;29:269–76.
[32] Juang HY, Hon MH. Fabrication and mechanical properties of hydroxyapatite-alumina composites. Mater Sci Eng C 1994;2:77–81.
[33] Viswanath B, Ravishankar N. Interfacial reactions in hydroxyapatite/alumina nanocomposites. Scr Mater 2006;55:863–6.
[34] Goldberg M, Smirnov V, Ievlev V, Barinov S, Kutsev S, Shibaeva T, et al. Influence of ripening time on the properties of hydroxyapatite-calcium carbonate powders. Inorg Mater 2012;48:181–6.
[35] Larson AC, Von Dreele RB. General structure analysis system (GSAS); report LAUR 86-748. Los Alamos, NM: Los Alamos National Laboratory; 2000.
[36] Toby BH. EXPGUI, a graphical user interface for GSAS. J Appl Cryst 2001;34(2):210–3.
[37] El Feki H, Savariault J-M, Ben Salah A. Structure refinements by the Rietveld method of partially substituted hydroxyapatite: $Ca_9Na_{0.5}(PO_4)_{4.5}(CO_3)_{1.5}(OH)_2$. J Alloys Compd 1999;287:114–20.
[38] Prodromou KP, Pavlatou-Ve AS. Formation of aluminum hydroxides as influenced by aluminum salts and bases. Clay Clay Miner 1995;43(1):111–5.
[39] Li H, Addai-Mensah J, Thomas JC, Gerson AR. The influence of Al (III) supersaturation and NaOH concentration on the rate of crystallization of $Al(OH)_3$ precursor particles from sodium aluminate solutions. J Colloid Interf Sci 2005;286(2):511–9.
[40] Wang M, Wang L, Shi C, Sun T, Zeng Y, Zhu Y. The crystal structure and chemical state of aluminum-doped hydroxyapatite by experimental and first principles calculation studies. Phys Chem Chem Phys 2016;18(31):21789–96.
[41] Goldberg MA, Smirnov VV, Protsenko PV, Antonova OS, Smirnov SV, Fomina AA, et al. Influence of aluminum substitutions on phase composition and morphology of β - tricalcium phosphate nanopowders. Ceram Int 2017;43:13881–4.
[42] Liu Y, Shen Z. Dehydroxylation of hydroxyapatite in dense bulk ceramics sintered by spark plasma sintering. J Eur Ceram Soc 2012;32:2691–6.
[43] Lazoryak BI, Strunenkova TV, Golubev VN, Vovk EA, Ivanov LN. Triple phosphates of calcium, sodium and trivalent elements with whitlockite-like structure. Mater Res Bull 1996;31:207–16.
[44] Shannon RD. Revised effective ionic radii and systematic studies of interatomic distances in halides and chalcogenides. Acta Crystallogr A 1976;32:751–67.
[45] Knowles JC, Gross K, Berndt CC, Bonfield W. Structural changes of thermally sprayed hydroxyapatite investigated by Rietveld analysis. Biomaterials 1996;17:639–45.
[46] Golubev VN, Viting BN, Dogadin OB, Lazoryak BI. Ca9M(PO4)7 (M = Al, Fe, Cr, Ga, Sc, Sb, In) binary phosphates. Rus J Inorg Chem 1990;35:3037–41.
[47] Gibson IR, Bonfield W. Novel synthesis and characterization of an AB-type carbonate-substituted hydroxyapatite. J Biomed Mater Res 2002;59(4):697–708.
[48] Mokhtari A, Belhouchet H, Guermat A. In situ high-temperature X-ray diffraction, FT-IR and thermal analysis studies of the reaction between natural hydroxyapatite and aluminum powder. J Therm Anal Calorim 2019;136(4):1515–26.
[49] Rau JV, Wu VM, Graziani V, Fadeeva IV, Fomin AS, Fosca M, et al. The bone building blues: self-hardening copper-doped

calcium phosphate cement and its in vitro assessment against mammalian cells and bacteria. Mater Sci Eng C Mater 2017;79:270–9.
[50] Chavda MA, Bernal SA, Apperley DC, Kinoshita H, Provis JL. Identification of the hydrate gel phases present in phosphate-modified calcium aluminate binders. Cement Concrete Res 2015;70:21–8.
[51] Garcia-Lodeiro I, Irisawa K, Jin F, Meguro Y, Kinoshita H. Reduction of water content in calcium aluminate cement with/out phosphate modification for alternative cementation technique. Cement Concrete Res 2018;109:243–53.
[52] Raynaud S, Champion E, Bernache-Assollant D, Thomas P. Calcium phosphate apatites with variable Ca/P atomic ratio I. Synthesis, characterization and thermal stability of powders. Biomaterials 2002;23(4):1065–72.
[53] Liao CJ, Lin FH, Chen KS, Sun JS. Thermal decomposition and reconstitution of hydroxyapatite in air atmosphere. Biomaterials 1999;20:1807–13.
[54] Mochales C, Wilson RM, Dowker SE, Ginebra MP. Dry mechanosynthesis of nanocrystalline calcium deficient hydroxyapatite: structural characterisation. J Alloys Compd 2011;509(27):7389–94.
[55] Elliott JC. Structure and chemistry of the apatites and other calcium orthophosphates. Stud Org Chem 1994;18, 94008066–94008066.
[56] Ahsan MR, Golam Mortuza M. Infrared spectra of xCaO (1– x– z) SiO_2zP_2O_5 glasses. J Non Cryst Solids 2005;351(27–29):2333–40.
[57] dos Santos ML, dos Santos Riccardi C, de Almeida Filho E, Guastaldi AC. Calcium phosphates of biological importance based coatings deposited on Ti-15Mo alloy modified by laser beam irradiation for dental and orthopedic applications. Ceram Int 2018;44(18):22432–8.
[58] Milev A, Kannangara GSK, Ben-Nissan B. Morphological stability of hydroxyapatite precursor. Mater Lett 2003;57(13–14):1960–5.
[59] Gupta A, Manohar CS, Siva Kumar B. Optimization of cation-doped nano-hydroxyapatite in combination with amorphous aluminum hydroxide for defluoridation. Water Supply 2019;19(6):1686–94, http://dx.doi.org/10.2166/ws.2019.041.
[60] Fisher DJ, McConnell D. Aluminum-rich apatite. Science 1969;164(3879):551–3.